

Effect of local strain on SCC initiation of Ni alloys

Danbi Song ^{a*}, Sung Woo Kim ^a, Dong Jin Kim ^a, Seong Sik Hwang ^a, Chang Hee Lee ^b

^a Nuclear Material Research Division, Korea Atomic Energy Research Institute,
Daedeok-Daero 989-111, Yuseong-Gu, Daejeon, Korea, 34057

^b Material Science and Engineering, Hanyang University,
222, Wangsimni-ro, Seongdong-gu, Seoul, Korea, 04763

*Corresponding author: dbsong@kaeri.re.kr

1. Introduction

Alloy 600 has been used traditionally for structural materials in nuclear power plants due to high resistance to general corrosion. However, there have been many localized corrosion failures in operating nuclear reactors. Most stress corrosion cracking (SCC) is an intergranular process along the grain boundaries. In order to design resistant materials or manage IGSCC by predicting the probability of failure during service, it is necessary to quantify the influences of GB characterization, strain and crystallography of the GBs on both crack initiation and propagation. Measuring the strain both in grains and at the GB is important for analyzing the initiation and propagation of the intergranular cracking. Electron backscatter diffraction (EBSD) is a high fidelity tool for providing the crystallographic information about the microstructure, Schmid factor and kernel average misorientation (KAM) value. The Schmid factor is the most widespread crystallographic parameter used to find the activated slip systems. The local strain distribution, meanwhile, was assessed using the KAM. The KAM is a local misorientation defined as an average misorientation of a point with all of its neighbors in grain.

In this study, crack initiation site was assessed by using the EBSD, then compared with in-situ monitored optical microscope images. Through these two methods microstructure and the micro-scale quantitative strain were analyzed. This work aims to observe crack initiation and propagation at all the grains using the in-situ optical microscope video image technique.

2. Experimental procedures

2.1 Materials and test specimen

Alloy 600 (heat no. 770177) steam generator tubing was used in this study and its chemical compositions are shown in Table 1. C-ring specimens were cut from tube with a 19.05 mm outer diameter (OD), 1.00 mm wall thickness. Specimens were prepared following ASTM standard G38-01, "Standard Practice for Making and Using C-ring Stress-Corrosion Test Specimens." [1]. Fig. 1 shows the schematic drawing of the unstressed (as-received) c-ring having an OD of 19.05 mm .

In order to achieve the sensitization of these specimens prior to experimental, all the specimens were thermally sensitized in N₂ gas at t 600 °C for 20 hours then air cooled. The materials were bending strained to 150 percent yield strength (Y.S) using an Alloy 600 bolts and nuts.

Table 1: chemical compositions of Alloy 600 (wt%)

C	Si	Mn	S	Cr	Ni	Fe	Cu
0.020	0.41	0.19	0.0005	16.29	73.0	9.45	0.010

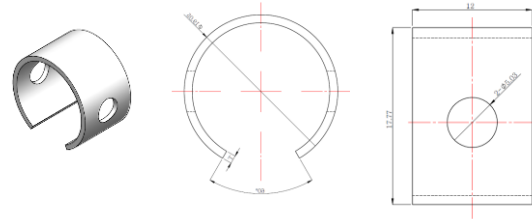


Fig.1. Schematic drawings of C-ring used in this work.

2.2 Electron backscattered diffraction examination

The EBSD scanning was performed on the flat side of c-ring in an area of around 350 μm x 350 μm on the specimens with a step size of 0.5 μm at magnification of 300 x and voltage of 15 KeV. Grain boundary characterization, Schmid factor, and the local strain distribution with the reduction of OD were analyzed with Hitachi SU5000 FE-SEM equipped with an EBSD instrument. The EBSD was in connection with TSL and Ch5 software for grain boundary characteristic and crystal orientation analysis.

2.3 In-situ monitoring with optical microscope

In-situ monitoring corrosion tests were carried out using specimens after EBSD analysis. SCC tests were performed in 0.1M sodium tetrathionate (Na₂S₄O₆) solution at room temperature [2], the well-known corrosive environment leading to IGSCC of the sensitized Ni-based alloy [2-3]. Specimen surfaces were micro shield coated remaining the EBSD analysis area. The crack initiation and propagation were video recorded for 3 to 7 days with optical microscope,

VOMS-100i lens x 1700 magnification, resolution of 1920 x 1080, and the frame rate of 29/sec.

3. Results and discussion

3.1. Characterization of microstructure and local strain

It was necessary to obtain OM images and compare them with the EBSD image in order to identify grain boundaries and crack initiation in the microstructure. Fig.2 (a) to through (e) show cracks propagation over time at magnification of 1700x with video optical microscope. Fig.3 shows the same area of the surrounding region where cracks initiated and propagated as shown Fig.2. The sequence of the cracks are shown in the Fig.2 (f). Fig.2 (f) is the KAM map obtained at the magnification of 300x of EBSD before SCC test. The red triangle represents the starting point of the crack. When the crack morphology is compared with KAM map, it is randomly initiated at highly strained region. Then it grows in a perpendicular direction to the stress, whereas direction of the stress suppresses crack progress. From these results, it can be seen that high local misorientation area on the grain boundary acts as crack initiation site. Then crack propagates along the high angle grain boundary, which is a typical corrosion type of alloy 600.

3.2. Grain boundary characterization and stress corrosion cracking

Fig.3. (a). shows image quality map with grain boundary characteristic using OIM software. The EBSD data are slightly cleaned up to show the grain boundaries more clearly. In this map, the red and green boundaries represent low-angle grain boundaries (LAGB, $2 < \theta < 5$, $5 < \theta < 15$), the blue boundaries represent random high angle grain boundaries (HAGB), and the yellow ones represent coincidence site lattice (CSL) which are called special boundaries. In this study, following Brandon's criterion was applied ($\Delta\theta = 15^\circ \Sigma^{-1/2}$) [4]. Fig.3(b) shows the CSL boundaries in more detail. It was treated using Ch5 software. In these maps the red, green, blue, pink, yellow boundaries are represented the $\Sigma 3$, $\Sigma 5$, $\Sigma 7$, $\Sigma 9$, $\Sigma 11$ respectively. In general, the special boundaries were considered to have great resistance to IGSCC because its lowest energy. In most cases, corrosion cracking susceptibility of alloy 600 decreases linearly with an increase in the fraction of the special boundary, especially with $\Sigma 3$ boundaries, which are more corrosion resistant [5-6]. In Alloy 600 and 690, the majority of CSL boundaries is $\Sigma 3$ twin boundaries, which were considered as the real special boundaries different from random boundaries.

In this study, mostly crack propagated along the HAGB. This results are in good agreement with other reserchers' results in therms of cack propagation [5-6].

The circle in Fig.3 (a) represents the CSL boundary. It can be seen that crack propagation to no.1 was suppressed by CSL boundary. Then the crack grows to no.2. The circles in Fig.3 (b) shows the cracks where the propagation is interrupted. It can be seen that the crack propagates along the grain boundary vertically to the stress direction.

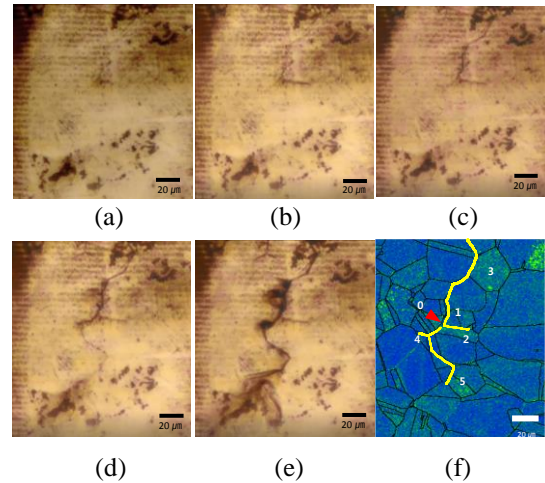


Fig.2. (a)- (e) Stereo-micrograph of crack progress (f) KAM image with crack sequence

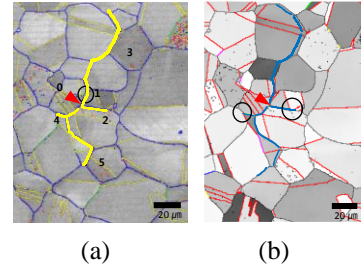
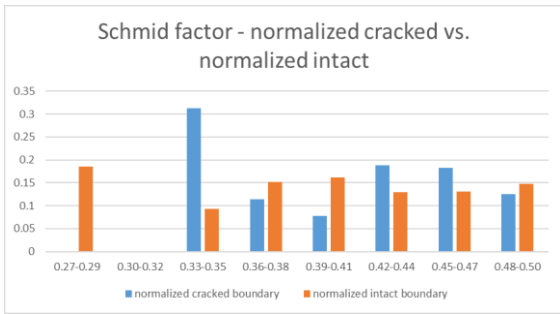


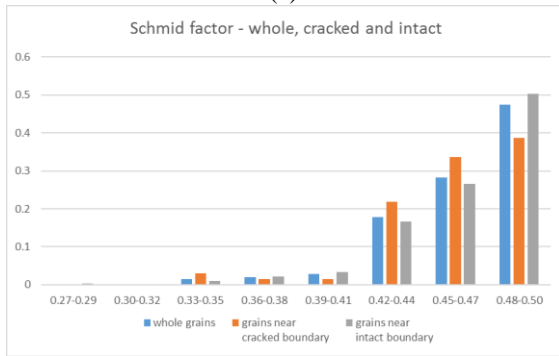
Fig. 3. (a) Map of image quality and grain boundary characterization (b) Schmid factor map with grain boundary characterization

3.3. Determining the crystallographic orientation using Schmid factor

The Schmid factor is the most widespread crystallographic parameter used to determine the activated slip systems in Ni-based alloys. Experimental techniques are available to directly measure the plastic strain heterogeneities that developed in polycrystalline materials, and have demonstrated that grains with higher Schmid factor tend to experience higher levels of strain than those with low Schmid factors [7-9]. However, as shown in the Figure 4, cracks do not necessarily occur as the Schmid factor value increase. Initiation and propagation of cracks are determined by several complex factors such as grain boundary engineering, local misorientation and crystallographic parameter.



(a)



(b)

Fig. 4. (a) Schmid factor distribution of whole grains, grain near cracked boundaries and grain near intact boundaries, (b) Normalized Schmid factor distribution with cracked boundaries and intact boundaries

4. Conclusions

This work aimed to investigate IGSCC initiation of Ni-based Alloys and its relationship with local strain, Schmid factor and GB character using in-situ technique with the aid of EBSD. It was found that crack first initiated at the highly strained surface and mostly grew along random high-angle grain boundaries. Cracks do not necessarily occur as the Schmid factor value increase.

REFERENCES

- [1] ASTM G38-01, Standard Practice for Making and Using C-ring Stress-Corrosion Test Specimens, Vol.03.02
- [2] S.-W. Kim, H.-P. Kim, J.-U.Jeong, and Y.-S. Chang, Effect of Residual Stress Of Dissimilar Metal Welding on Stress Corrosion Cracking of Bottom Mounted Instrumentation Penetration Mock-Up, Corrosion, 66 (2010) 106001-1~106001-8.
- [3] HUH G. H. HOROWITZ, Chemical Studies of Polythionic Acid Stress Corrosion Cracking, Corrosion science, 23 (1983) 353-362.
- [4] D.G BRANDON, The structure of high angle grain boundaries, Acta metallurgica, 14 (1966) 1479-1484.
- [5] J.Hou, T.Shoji, Z.P.Lu, Q.J.Wang, E.-H.Han, W.ke, Residual strain measurement and grain boundary characterization in the heat-affected zone of a weld joint between Alloy 690TT and Alloy 52, Journal of nuclear materials, 397 (2010) 109-115.
- [6] J.Hou, Q.J. Peng, Z.P. Lu, T.Shoji, J.Q. Wang, E.-H. Han, and W.Ke, Effects of cold working degrees on grain

boundary characters and strain concentration at grain boundaries in Alloy 600, Corrosion science, 53 (2011) 1137-1142.

- [7] Alisa Stratulat, Jonathan A. Duff, T.James Marrow, Grain boundary structure and intergranular stress corrosion crack initiation in high temperature water of a thermally sensitized austenitic stainless steel, observed in situ, Corrosion science, 85 (2014) 428-435.
- [8] E.A. West, G.S. Was, A model for the normal stress dependence of intergranular cracking of irradiated 316L stainless steel in supercritical water, Journal of nuclear materials, 408 (2011) 142-152.
- [9] A. Clair, M. Foucault, O.Calonne, Y.Lacroute, L.Markey, M. Salazar, V.Vignal, E.Fiot, Strain mapping near a triple junction in strained Ni-based alloy using EBSD and biaxial nanogauges, Acta marerialia, 59 (2011) 3116-3123.